The Astrophysical Journal, 812:150 (9pp), 2015 October 20 doi:10.1088/0004-637X/812/2/150

ICE CHEMISTRY ON OUTER SOLAR SYSTEM BODIES: ELECTRON RADIOLYSIS OF N_2-, CH_4-, AND CO-CONTAINING ICES

Christopher K. Materese[1,2], Dale P. Cruikshank[1], Scott A. Sandford[1], Hiroshi Imanaka[1,3], and Michel Nuevo[1,4]
[1] NASA Ames Research Center, MS 245-6, Moffett Field, CA 94035-1000, USA
[2] Oak Ridge Associated Universities, P.O. Box 117, MS 36, Oak Ridge, TN 37831-0117, USA
[3] SETI Institute, 189 N. Bernardo Ave., Suite 100, Mountain View, CA 94043, USA
[4] Bay Area Environmental Research Institute, 625 2nd St., Suite 209, Petaluma, CA 94952, USA
Received 2015 May 13; accepted 2015 September 2; published 2015 October 20

ABSTRACT

Radiation processing of the surface ices of outer Solar System bodies may be an important process for the production of complex chemical species. The refractory materials resulting from radiation processing of known ices are thought to impart to them a red or brown color, as perceived in the visible spectral region. In this work, we analyzed the refractory materials produced from the 1.2-keV electron bombardment of low-temperature N_2-, CH_4-, and CO-containing ices (100:1:1), which simulates the radiation from the secondary electrons produced by cosmic ray bombardment of the surface ices of Pluto. Despite starting with extremely simple ices dominated by N_2, electron irradiation processing results in the production of refractory material with complex oxygen- and nitrogen-bearing organic molecules. These refractory materials were studied at room temperature using multiple analytical techniques including Fourier-transform infrared spectroscopy, X-ray absorption near-edge structure (XANES) spectroscopy, and gas chromatography coupled with mass spectrometry (GC-MS). Infrared spectra of the refractory material suggest the presence of alcohols, carboxylic acids, ketones, aldehydes, amines, and nitriles. XANES spectra of the material indicate the presence of carboxyl groups, amides, urea, and nitriles, and are thus consistent with the IR data. Atomic abundance ratios for the bulk composition of these residues from XANES analysis show that the organic residues are extremely N-rich, having ratios of $N/C \sim 0.9$ and $O/C \sim 0.2$. Finally, GC-MS data reveal that the residues contain urea as well as numerous carboxylic acids, some of which are of interest for prebiotic and biological chemistries.

Key words: astrochemistry – Kuiper Belt: general – molecular data – molecular processes – planets and satellites: surfaces – solid state: refractory

1. INTRODUCTION

Transneptunian objects (TNOs) orbit the Sun beyond Neptune in the region between 30 to several hundred astronomical units where ices are predominant. TNOs are thought to be some of the most primitive bodies in the Solar System but detailed information about their physical properties has been difficult to obtain because of their relatively small sizes, low albedos, and large distances from Earth. The arrival of the *New Horizons* spacecraft at the Plutonian system in 2015 July provided the first opportunity to examine these objects in detail (Stern 2008; Young et al. 2008).

Pluto, one of the largest TNOs, is a cold world, with much of its surface covered with ice. Specifically, spectroscopic data have shown that Pluto's surface ice is dominated by N_2, CH_4, and CO. Small quantities of other ices such as C_2H_6 have also been detected (Cruikshank et al. 2006; DeMeo et al. 2010; Cook et al. 2014). Notably, Pluto exhibits significant surface variegation, which may in part be the result of the presence of complex organic molecules. Despite the frigid temperatures, these complex organic molecules were likely produced through chemical reactions in the atmosphere and in surface ices through radiation processing.

In ices, radiation processing leads to the production of ions and radicals that may react with their neighbors to form new species (d'Hendecourt et al. 1986; Allamandola et al. 1988; Gerakines et al. 2001; Baragiola et al. 2013). Additionally, some of these radicals may remain trapped until the surrounding ice matrix changes, as may occur seasonally on Pluto's surface. The chemistry that results from these processes is largely driven by kinetics and will therefore not necessarily yield the most thermodynamically favorable product. Consequently, the radiation processing of ices can yield products that are far more complex than the initial reactants, and these products will not necessarily be in chemical equilibrium.

At Pluto's orbit, UV radiation from the Sun is the most abundant source of ionizing radiation available to drive chemistry in ices, exceeding the galactic cosmic ray flux in terms of energy by a factor of $\sim 10^5$ (Madey et al. 2002). However, the atmosphere of Pluto is currently optically thick with respect to energetic Lyα photons. Consequently, at the present time Lyα only drives gas-phase reactions in Pluto's upper atmosphere and has vanishingly little influence on the surface ices, while radiation processing of Pluto's surface is currently primarily driven by energetic particle bombardment (e.g., cosmic rays). Despite their large energies, cosmic rays can only interact with the matter they pass through in much smaller, discrete, quantized steps. Indeed, much of the energy deposited in the ices by cosmic rays is dispersed in the form of secondary electrons that drive much of the resulting chemistry (Hudson et al. 2008). It should be noted that the column density of Pluto's atmosphere may change significantly over the planet's seasonal cycle (Lellouch et al. 2009). Changes in the density of Pluto's atmosphere may mean that the dominant form of energetic processing of the surface ice could change with time, with UV radiation becoming more important at the surface during times when Pluto's atmosphere is thinnest. Because of this, UV radiation and energetic particles may both

play an important role in the in ice chemistry on Pluto's surface.

Laboratory experiments can provide important insights into the chemistry that may occur on the surface of Pluto and other TNOs. For example, the use of simple ice analogs has provided significant insight into the identity of many small molecules produced by the radiation processing of ices relevant to TNOs (Bohn et al. 1994; Moore & Hudson 2003; Hodyss et al. 2011; Kim & Kaiser 2012; Wu et al. 2012, 2013). Additionally, some work has already been done to study the refractory residues using infrared spectroscopy of similar ices subjected to ion bombardment (Strazzulla et al. 2001; Palumbo et al. 2004). Recently, we studied the UV photoprocessing of Pluto-like ice mixtures with a focus on the resulting refractory materials (Materese et al. 2014).

In this paper, we use the 1.2-keV electron (e^-) irradiation of mixed N_2, CH_4, and CO ices to model the cosmic ray bombardment of the surface of Pluto and other TNOs with similar surface ice composition, which is appropriate for the radiation exposure currently being experienced by ices on Pluto. For comparison purposes, we repeated some of our previous experiments with UV photons as the radiation source using the same equipment and conditions as was used for the e^- experiments. It should be noted that there were no major differences in the UV-irradiated residues produced for this work from those previously published in Materese et al. (2014). This paper focuses on the properties of the refractory residues that result from these irradiation experiments using multiple analytical techniques, including FTIR spectroscopy (mid- and near-IR regions, from 7000 to 600 cm^{-1}, 1.43–16.7 μm), X-ray absorption near-edge structure (XANES) spectroscopy, and gas chromatography coupled with mass spectroscopy (GC-MS). The properties of the residues from the UV- and e^--irradiated ices are also compared to samples of poly-HCN provided by Bob Minard (Minard et al. 1998) and later analyzed by Hiroshi Imanaka (Imanaka & Smith 2010). Poly-HCN has been suggested as a possible component of the refractory carbonaceous material found on comets and on the surfaces of objects in the outer Solar System (e.g., Cruikshank et al. 1991; Matthews 1992) and has been previously compared to Titan-like tholins produced in the laboratory (Vuitton et al. 2010).

2. RESULTS

All experimental methods are presented in the Appendix. Irradiation of N_2:CH_4:CO ice mixtures at 15–20 K with 1.2-keV e^- produced ions and radicals in the ice. As previously stated, some of these ions and radicals reacted immediately with their neighbors in the ice matrix to form new products. As the samples were subsequently warmed, many of the remaining unreacted ions and radicals trapped in the ice matrix became mobilized, allowing them to react. Most of the ice matrix sublimes from 35 to 50 K, meaning most ions and radicals react during before or during this temperature interval. Little new chemistry is expected to occur after this phase of the warm-up, although many of the more volatile products may be lost before reaching room temperature. After the volatile compounds had completely sublimed, a refractory organic residue remained at 300 K, and was collected for analysis with IR spectroscopy, XANES, and GC-MS.

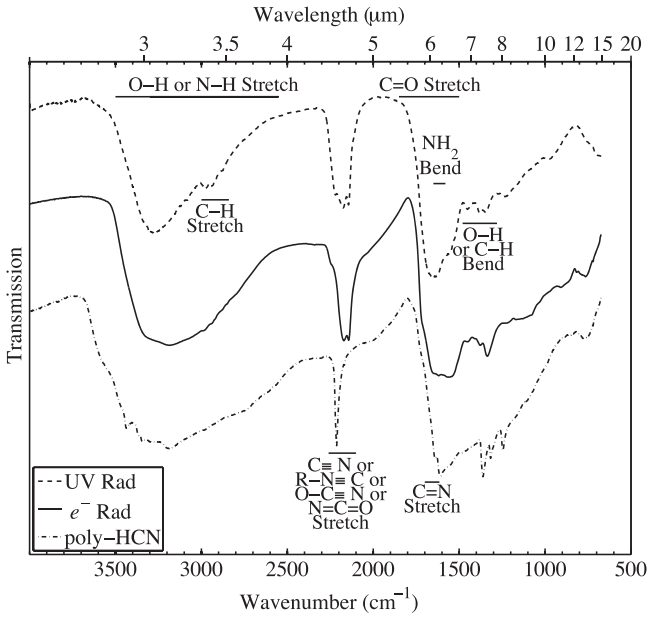

Figure 1. Normalized mid-infrared spectra of the refractory residues from UV- and e^--irradiated ice mixtures, in addition to a sample of poly-HCN. Un-scaled C≡N related bands in each spectrum were approximately 90%, 70%, and 96% transmission for the UV-, e^--irradiated, and poly-HCN samples, respectively.

2.1. Infrared Spectroscopy

The mid-IR spectra (4000–600 cm^{-1}, 2.50–16.7 μm) of refractory residues produced from the e^- irradiation of N_2:CH_4:CO ices can be compared with those produced from the UV irradiation of the same ice mixtures as well as a sample of poly-HCN (Figure 1). There is generic similarity in the infrared spectra of all three of these samples, suggesting they contain many of the same functional groups. Infrared spectra of the residues resulting from both UV and e^- irradiated ices were taken immediately after extraction from the vacuum chambers and then later at varying intervals for over a month. Both types of residues appear to be relatively chemically stable at room temperature, with no major changes observed in the infrared spectra during this time.

The UV- and e^--irradiated residues both have a broad absorption feature between 3600 and 2400 cm^{-1} (2.78–4.17 μm) that is consistent with the overlapping of O–H and N–H stretching modes. In comparison, the poly-HCN sample has a broader feature that falls between 3700 and 2300 cm^{-1} (2.70–4.35 μm). In the UV-irradiated samples, C–H stretching modes appear between 3000 and 2750 cm^{-1} (3.33–3.63 μm) but are notably weaker in the e^- irradiated and poly-HCN samples. In both the UV-and e^--irradiated samples, a strong feature with multiple peaks appears between 2300 and 2050 cm^{-1} (4.35–4.87 μm) that is consistent with C≡N, O–C≡N, or N=C=O moieties (Imanaka et al. 2004). In the UV-irradiated sample, these peaks fall at 2220 cm^{-1} (4.50 μm), 2175 cm^{-1} (4.60 μm), and 2145 cm^{-1} (4.66 μm). In the e^--irradiated sample, a shoulder appears near 2245 cm^{-1} and the main peaks fall at 2172 cm^{-1} (4.60 μm) and 2143 cm^{-1} (4.67 μm). These features may be consistent with the presence of various nitriles, isonitriles, cyanates, and/or isocyanates. Notably, the poly-HCN sample also has a much narrower feature in this region with one large peak at 2213 cm^{-1}

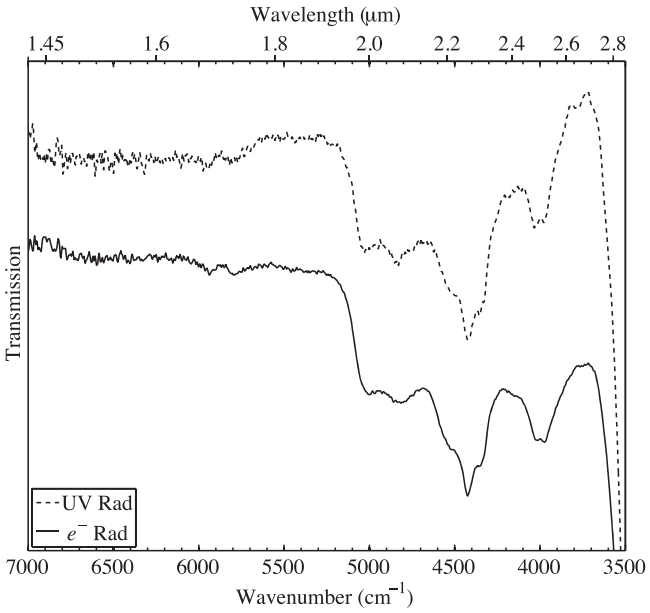

Figure 2. Near-infrared spectra of the refractory residues from UV- and e^--irradiated ice mixtures.

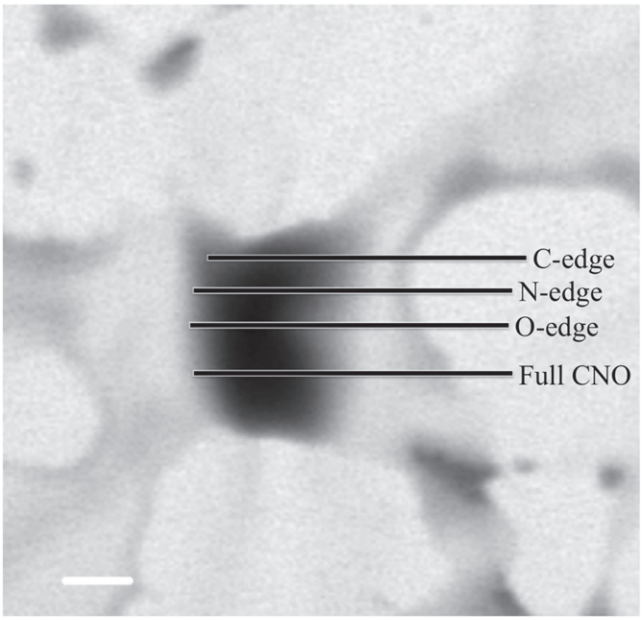

Figure 3. X-ray absorption image (390 eV) of a portion of the refractory residue produced from an e^--irradiated ice sample. Lines are 10 μm in length and indicate the locations where the various scans were taken.

(4.52 μm) and a small shoulder at 2168 cm^{-1} (4.61 μm). This feature can be attributed to the nitriles present in the poly-HCN sample.

The UV-irradiated sample shows a peak at 1650 cm^{-1} (6.06 μm), a large shoulder near 1555 cm^{-1} (6.43 μm), a small shoulder near 1524 cm^{-1} (6.56 μm), and a peak near 1450 cm^{-1} (6.90 μm), while the e^--irradiated sample has a shoulder near 1717 cm^{-1} (5.82 μm), and peaks at 1649 cm^{-1} (6.06 μm), 1618 cm^{-1} (6.18 μm), 1555 cm^{-1} (6.43 μm), and near 1450 cm^{-1} (6.90 μm). These bands are consistent with the presence of C=O or C=N stretching modes as well as NH or NH_2 bending modes. The poly-HCN sample differs significantly from the UV- and e^--irradiated samples over this region of the IR spectrum, showing much less absorption in the 1800–1650 cm^{-1} (5.56–6.06 μm) range. The peaks of the poly-HCN sample falling in this spectral region are at 1639 cm^{-1} (6.10 μm) and 1607 cm^{-1} (6.22 μm).

Finally, both the UV-and e^--irradiated samples have a series of unidentified bands near 1410 cm^{-1} (7.09 μm), 1380 cm^{-1} (7.25 μm), 1340 cm^{-1} (7.46 μm), and 1227 cm^{-1} (8.15 μm). The profile of the poly-HCN sample bears little similarity to that of the UV-and e^--irradiated samples in the 1450–830 cm^{-1} (6.90–12.0 μm) region. Both the poly-HCN sample and the e^--irradiated samples have similar broad absorptions bands centered near 760 cm^{-1} (13.2 μm) that are consistent with the N–H out of plane wagging modes in primary amides.

Near-IR spectra (7000–4000 cm^{-1}, 1.43–2.50 μm) were also collected independently for both UV- and e^--irradiated residues (Figure 2). This spectral region is accessible to Earth-based spectroscopy of Pluto and related objects (e.g., Grundy et al. 2013), and is also covered by the LEISA spectrometer on board the *New Horizons* spacecraft, which encountered Pluto and its satellites in 2015 July (Young et al. 2008). The laboratory spectra and identifications presented here will inform the analysis of infrared spectroscopy of Pluto and related objects, with particular emphasis on the non-ice component(s) of their surfaces.

As shown in Figure 2, the near-IR spectra of these two residues are nearly indistinguishable. The features in this spectral range are all due to combination and overtone vibrational modes of the same chemical subgroups whose fundamentals are seen in the mid-IR. Weak absorptions in the residues at 5938 and 5790 cm^{-1} (1.68 and 1.73 μm) are consistent with C–H stretching combination modes. A doublet appears near 5000 cm^{-1} (2.00 μm), consistent with N–H stretch and NH_2 scissoring combination modes in primary amines or amides (Cruikshank et al. 2005). The next major feature contains several overlapping peaks, the first of which is observed near 4530 cm^{-1} (2.21 μm) is consistent with an amide combination mode ($2\nu_{C=O}$ + amide NH_2 bending mode). Finally, there is a peak at 4426 cm^{-1} (2.26 μm) and a shoulder at 4359 cm^{-1} (2.29 μm) consistent with C≡N or O–C≡N overtones, respectively.

2.2. XANES Spectroscopy

Like IR spectroscopy, XANES is a valuable tool that provides information about the chemical bonds present in a sample. This technique can be used as a verification for interpretation of the IR spectra and may also provide new insight for identifying otherwise ambiguous IR spectral features. Residues are prepared on grids designed for transmission electron microscopy (TEM), made of copper and covered with a SiO film that is nearly transparent at the X-ray energies used to image the sample. To avoid beam saturation, it is necessary to locate an optically thin portion of the sample on the XANES sample holder while maintaining good signal to noise. To accomplish this, increasingly magnified X-ray images of the TEM grid were collected until potentially suitable areas of each sample could be chosen.

Figure 3 shows a representative X-ray absorption image (390 eV) of an e^--irradiated sample selected for the XANES measurements. The lines on this image correspond to the locations where XANES line scans were taken across the C, N,

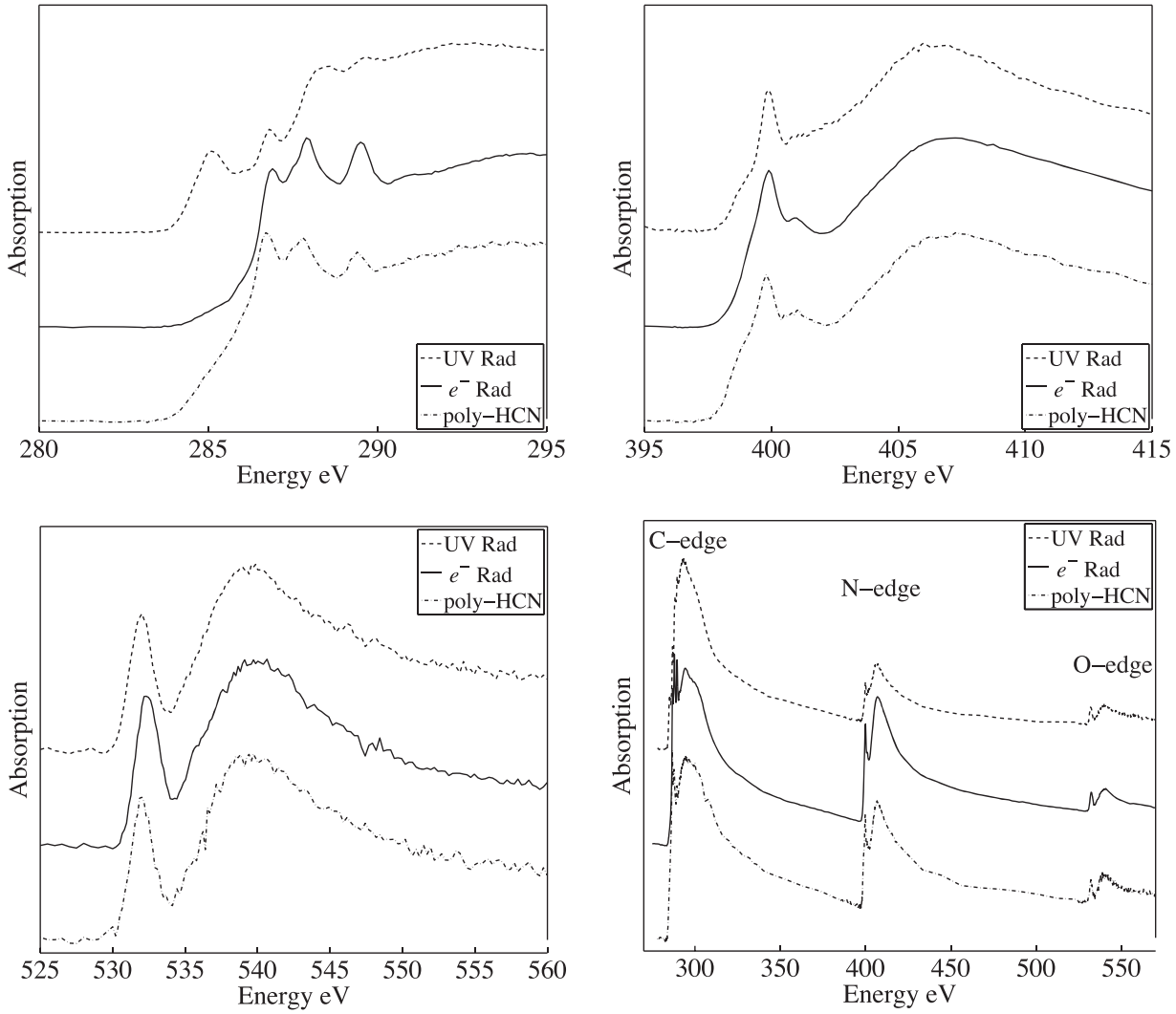

Figure 4. XANES carbon (top left), nitrogen (top right), and oxygen (bottom left) edges in addition to full CNO scans (bottom right) of residues from UV- and e^--irradiated ices as well as a poly-HCN sample.

Table 1
X-ray Absorption Features Detected in a Typical Refractory Residue

Edge	Sample Type	Energy (eV)[a]	Functional Group	Transition
C edge	UV, e^- (sh), poly-HCN (sh)	285.2	aromatic/olefinic: C=C*	1s-π^*
	UV, e^-, poly-HCN	286.7–286.9	nitrile: C*≡N	1s-π^*
	UV (sh), e^-, poly-HCN	287.9	amide: N–C*=O	1s-π^*
	UV	288.4–288.7	carboxyl: OR(C*=O)C	1s-π^*
	UV, e^-, poly-HCN	289.4–289.8	urea: $NH_x(C^* = O)NH_x$ or alcohol/ether: CH_x–OR	1s-π^* or 1s-3p/s*
N edge	UV, e^-, poly-HCN	399.9	nitrile: C≡N*	1s-π^*
	e^-, poly-HCN	401.0	amide: N*–C=O	1s-π^*
O edge	UV, e^-, poly-HCN	532.0	carboxyl: O–C=O* or amide: N–C=O*	1s-π^*

Note.
[a] Energies from Gordon et al. (2003), Cody et al. (2008), and De Gregorio et al. (2011); (sh) indicates that the feature appears as a shoulder.

and O edges. C-, N-, and O-edge spectra and complete CNO spectra of residues from both the UV- and e^--irradiated ices and a sample of poly-HCN are shown in Figure 4. Based on previous XANES energy assignments (Gordon et al. 2003; Cody et al. 2008; De Gregorio et al. 2011), the bands seen in these spectra have been assigned to the specific functional

Table 2
Complete List of Compounds Identified by GC-MS from the Residues of both UV- and e^--irradiated N_2:CH_4:CO Ices

Name/Formula	Retention Time (R_t)	Mass	Presence in Sample
Lactic acid ($C_3H_6O_3$)	14.7	261	UV
Glycolic acid ($C_2H_4O_3$)	15.1	247	UV, e^-
Oxalic acid ($C_2H_2O_4$)	16.0	261	UV
2-Hydroxybutyric acid ($C_4H_8O_3$)	16.4	279	UV
3-Hydroxypropionic acid ($C_3H_6O_3$)	16.7	261	UV, e^-
Urea (CH_4N_2O)	18.5	231	UV, e^-
Glyceric acid ($C_3H_6O_4$)	25.0	394	UV

groups listed in Table 1. There are significant differences between the C- and N-edge spectra from the UV- and e^--irradiated samples, however, the e^--irradiated and poly-HCN samples are remarkably similar (Figure 4). The C-edge spectrum of the UV-irradiated sample has a peak that is consistent with the presence of aromatic and/or olefinic C=C bonds (285.2 eV). In contrast, there is only a small shoulder matching this feature in the e^--irradiated and poly-HCN samples. All three samples possess strong bands indicative of the presence of nitrile (C≡N) moieties in both their C- and N-edge spectra (286.7–286.9 eV and 399.9 eV, respectively). The C-, N-, and O-edge spectra of the e^--irradiated and poly-HCN samples also possess peaks consistent with the presence of amide moieties (287.9 eV, 401 eV, and 532.0 eV respectively). In the UV-irradiated ice, the C- and O-edge spectra are consistent with the presence of carboxyl groups (288.4–288.7 eV and 532.0 eV, respectively), but no corresponding bands are detectable in the e^--irradiated or poly-HCN samples. Finally, all three samples show peaks in the carbon edge between 289.4–289.8 eV that are consistent with urea, alcohols, ethers, or some mixture of those; however, no corresponding peaks were identified in the N or O edges.

The relative elemental abundances of C, N, and O in our samples can be estimated by comparing the increase in absorption above the associated ionization edge to the absorption below the ionization edge (Cody et al. 2008; Nuevo et al. 2011; Materese et al. 2014). Specifically, estimated N/C and O/C ratios were obtained by fitting the full CNO spectra with atomic absorption coefficients (Henke et al. 1993) using the model described in Cody et al. (2008). Imanaka and Smith (2010) previously determined a N/C ratio of 0.93 for the poly-HCN sample using combustion elemental analysis. This is consistent with the XANES determination of a N/C ratio of ∼0.9. As previously reported, the UV-irradiated samples show N/C and O/C ratios of ∼0.5 and ∼0.3, respectively (Materese et al. 2014). However, the e^--irradiated samples contain significantly more nitrogen, with N/C and O/C ratios ∼0.9 and ∼0.2, respectively. As was the case with our previous samples, more accurate ratios could not be determined because of deviations from tabulated photoabsorption curves likely caused by scattering effects. The high N/C ratios measured for residues produced from e^--irradiated ice are consistent with the absence of CH_3/CH_2 stretching bands in its mid-IR spectra, as most of the carbon may be bound to nitrogen atoms to form nitriles and other C–N bonds, preventing the formation of long aliphatic chains.

2.3. GC-MS

After the IR spectra of the samples were collected, the residues produced on aluminum foils were analyzed using GC-MS. Sample residues were extracted from the foils using either a 1:1 mixture of acetonitrile and methanol, or a solution containing the derivatization agent MTBSTFA. Both derivatized and underivatized samples were injected into the GC-MS, but only the chromatograms from the former yielded any identifiable compounds (Table 2). Additionally, a derivatized sample and an underivatized sample of poly-HCN were injected into the GC-MS, but no identifiable peaks were present in the chromatograms. Chromatograms of derivatized samples for both UV- and e^--irradiated samples contained many peaks, of which only a few could be identified using our in house standards and the NIST database. As previously reported, the UV-irradiated samples contained lactic acid, glycolic acid, oxalic acid, 2-hydroxybutyric acid, 3-hydroxypropionic acid, glyceric acid, and urea (Materese et al. 2014). Similarly, e^--irradiated samples contain lactic acid, glycolic acid, 3-hydroxypropionic acid, oxalic acid, and urea. However, some of these had been previously shown to appear in blank samples containing only the derivatization agent, but no residue (Materese et al. 2014). In order to verify that the identified molecules were actually products of e^- bombardment in our ice analogs, the experiments were repeated using CO with isotopically labeled oxygen ($C^{18}O$) in the starting ice mixture. Isotopic labeling experiments were only able to confirm the production of glycolic acid, 3-hydroxypropionic acid, and urea.

Mass spectra of the 3 compounds identified in the e^--irradiated residues are shown in Figure 5. Their abundances were estimated by comparing the integrated band intensities in the chromatograms of a given sample with those in the chromatogram of standards of known concentration. The carboxylic acids in the e^--irradiated samples appeared as relatively small peaks in the chromatogram and were estimated to have abundances of ∼0.1 nmol. The peak identified as urea was the largest in the sample and was estimated to have an abundance of ∼5 nmol. These data indicate a ratio of approximately 50 to 1 for urea molecules to individual carboxylic acids in the e^--irradiated samples, in contrast to the 1 to 2 (or more) ratio for urea to individual carboxylic acids in the UV-irradiated samples (Materese et al. 2014). Altogether, these data suggest that relative to the carboxylic acids in the samples, urea is over 100 times more abundant in residues produced by e^- bombardment than it is in residues produced from UV photons.

It should be noted that the main background contaminant in our vacuum systems is H_2O. As reported in our previous work, H_2O accounts for ∼0.05% of the total ice in one of these experiments (Materese et al. 2014). Since CO is the only source of oxygen intentionally added to our ices, the use of isotopically labeled $C^{18}O$ provides a means to gauge how much of the oxygen contained in our final residues comes from unintended sources including contaminant H_2O. Our GC-MS data suggest that 75% of the oxygen contained in the residues comes from the CO in the initial ice mixture, while the remaining 25% comes from one or more other sources. This suggests that the oxygen from the contaminant H_2O can also be incorporated into the final residue, likely increasing the relative abundance of oxygenated compounds compared to residues that would be produced from an ice devoid of H_2O. It should be

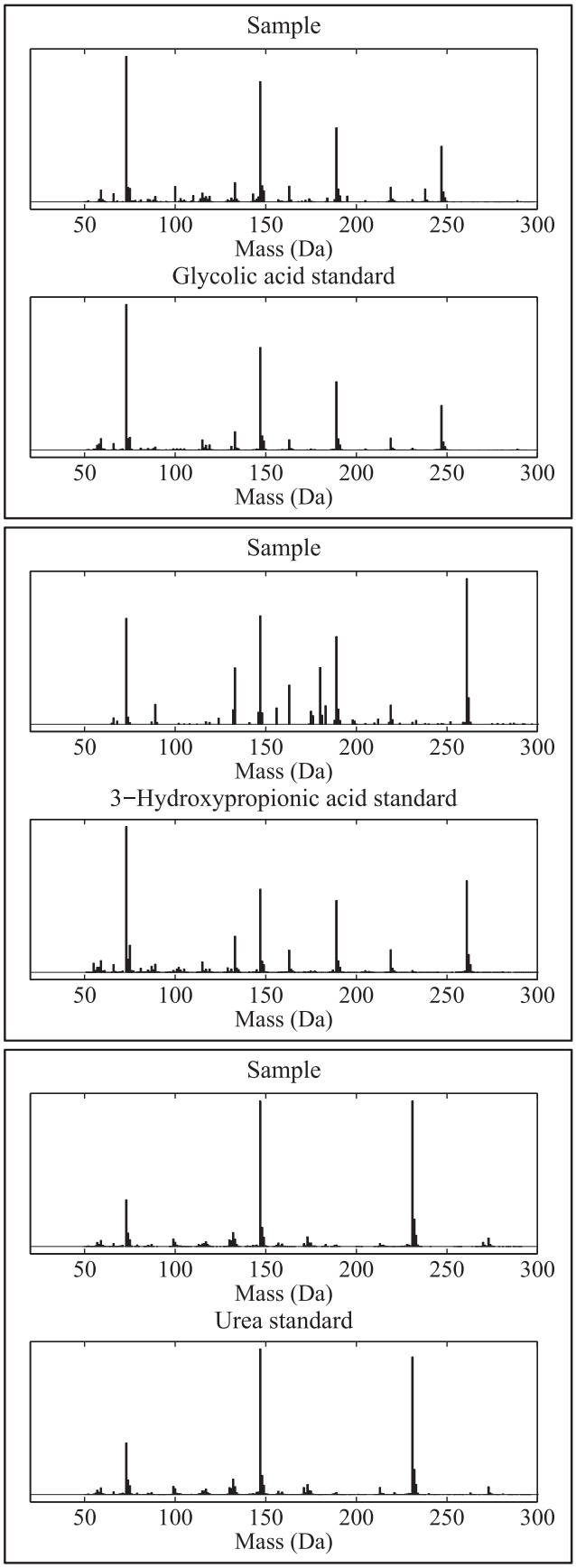

Figure 5. Mass spectra of the three identified compounds in the refractory residues produced by the e^--irradiated ice mixtures.

noted that the contaminant oxygen is more likely to have originated from contaminant water rather than from oxygen in the atmosphere because of the apparent stability of the residues at room temperature as inferred from the infrared spectra. Regardless, glycolic acid, 3-hydroxypropionic acid, and urea are all shown to be produced in part using only oxygen derived from $C^{18}O$. This suggests that while the relative abundances of product molecules may change, the overall chemistry observed is relatively insensitive to the presence of small quantities of H_2O.

3. DISCUSSION

The data collected in these experiments overwhelmingly indicate that the e^--bombardment of Pluto ice analogs produces a highly nitrogen-rich complex organic residue. This residue is significantly more nitrogen-rich than the residues produced from the same ices if UV is the primary energy source (Materese et al. 2014). This is likely the result of the greater efficiency with which 1.2-keV electrons can break the strong N≡N bond in N_2 compared to Lyα photons. This finding is strongly supported by the IR and XANES data and also suggested by the GC-MS results.

While the abundance of individual molecules may vary between samples, the high N/C ratio (∼0.9) of the bulk material in the e^--irradiated residues is important because it greatly limits the options for possible functional groups, which has important consequences that can be detected spectrally. For example, such a high N/C ratio greatly limits the number of methylene groups (CH_2) that can be present. The result of this is clearly seen with the weakness of the CH_2 stretching modes in the IR spectra of the e^--irradiated samples compared to the UV-irradiated samples (Materese et al. 2014). Since the samples also contain modest quantities of oxygen (O/C ∼ 0.2), it also suggests that there is likely little room for terminal methyl groups (–CH_3), which are not detected in the IR spectra either. Another consequence of the high N/C ratio is that there should be fewer carbons directly bonded to other carbons in the residue, which is consistent with the weakness of the C=C feature in the XANES data. The greater abundance of amide moieties as detected by the XANES data in the e^--irradiated samples in contrast to the greater abundance of carboxyl groups in the UV irradiated samples also appears to be consistent with increased N incorporation. In the GC-MS samples, the relative abundance of urea (a nitrogen bearing compound), compared to carboxylic acids (non-nitrogen bearing compounds), was shown to increase by a factor of over 100 in residues processed by e^- irradiation compared to residues irradiated with UV photons, further demonstrating the increased dominance of nitrogen bearing species.

The XANES spectra of residues from e^--irradiated ices are very similar to those of poly-HCN. Despite these similarities, there are notable differences in the mid-IR spectra of poly-HCN and the residues from both UV- and e^--irradiated ices. One notable difference is the relative simplicity and narrowness of the C≡N feature in the poly-HCN sample. The simplicity of this feature suggests that the C≡N moieties in poly-HCN are more uniform and in more chemically similar environments than those found in either of the experimental samples. Consequently, this suggests that both UV- and e^--derived experimental samples are more chemically complex than poly-HCN, despite similarities in many of the types of functional groups present. This is similar to the results of Vuitton et al.

(2010), who found that poly-HCN was chemically simpler than laboratory derived Titan-like tholins.

The near-IR data reported in this study show spectral features within the range of detection of the *New Horizons* spacecraft (Young et al. 2008). If the types of complex organic materials produced in these laboratory experiments are representative of those found on Pluto's surface and if they are sufficiently abundant, then we could reasonably expect that some of the bands reported in this work will be found in the *New Horizons* spectral data after the contributions of the strongly absorbing ices are accounted for. Unfortunately, this wavelength region does not appear to be highly diagnostic as to which radiation source (UV or particle) produced these complex organic residues.

Despite this, understanding the chemistries that result from both particle bombardment and UV photolysis is important for understanding the surface compositions of TNOs with little to no atmosphere. Even for objects that currently have an atmosphere that is optically thick with respect to high energy UV radiation like Lyα (e.g., Pluto), an understanding of both chemistries may still be important. On these objects, particle bombardment is currently the most important source of energetic processing of the surface ice. However, if such an object undergoes significant seasonal variations in the density of the atmosphere, or if the object experienced a historic atmospheric collapse on the timescale of the age of its surface, it may have experienced a regime in which UV photolysis dominated.

4. CONCLUSION

Complex organic residues similar to those produced in our laboratory experiments might contribute significantly to the non-ice components on the surface of Pluto. Previously, we characterized the composition of refractory residues produced by the UV photolysis of Pluto-like ices. In this paper, we show the similarities and differences between residues produced through the UV photolysis and those produced from e^- irradiation of those ices. Notably, a major difference in the resulting residues produced from these two radiation sources is the level of nitrogen incorporation ($N/C \sim 0.5$ for UV, $N/C \sim 0.9$ for e^-). This is probably due to the fact that Lyα UV photons are not as efficient at breaking the strong N≡N bond as are 1.2-keV electrons. The high level of nitrogen incorporation in the residues produced from e^--irradiated ices has the interesting consequence that it puts strong limits on the abundances of various functional groups that involve C–C bonds (e.g., CH_2, CH_3, C=C, etc.).

Notably, residues derived from both UV- and e^- irradiation show generic similarities to poly-HCN in their mid-IR spectra. A comparison of all three using XANES spectroscopy demonstrates that the e^--irradiated sample is extremely similar to poly-HCN, while both have notable differences from the UV-irradiated sample. Overall, the data appear to indicate that poly-HCN is chemically simpler than both the UV-irradiated and e^--irradiated samples.

An understanding of the chemistry driven by both UV photoprocessing and particle bombardment may be important to fully understand the surface compositions of icy TNOs like Pluto regardless of the opacity of their atmosphere to UV photons. This is because these bodies may undergo seasonal variations in the density of their atmospheres that may allow high-energy ionizing UV photons to reach the surface. Alternatively, both radiation sources may be important if the object experienced a historical collapse of the atmosphere on a timescale comparable to the age of the surface.

Finally, the *New Horizons* spacecraft will provide detailed measurements of the surface composition of Pluto in the near-IR range from 1.25 to 2.5 μm, which will be compared to the near-IR spectra measured for our residues. Specifically, the residues produced from our experiments possessed peaks at 1.68 and 1.73 μm, a doublet near 2 μm, series of overlapping peaks from 2.1 to 2.3 μm (2.21, 2.26 μm, and a shoulder at 2.29 μm), and a doublet near 2.5 μm. We predict that if the residues produced in these experiments are representative of the complex organics found on Pluto and make a significant contribution to its surface composition, then these bands may be observable in the *New Horizons* data.

C.K.M. acknowledges R.L. Walker (NASA Ames) for technical support, the NASA Postdoctoral Program (NPP) administered by ORAU, and D. Kilcoyne for assistance with ALS beamline 5.3.2.2. D.P.C. acknowledges support from NASA's New Horizons mission program. H.I. acknowledges supports from NASA's Cassini Data Analysis Program. This material is based on work supported by the National Aeronautics and Space Administration through the NASA Astrobiology Institute under Cooperative Agreement Notice NNH13ZDA017C issued through the Science Mission Directorate. The Advanced Light Source is supported by the Director, Office of Science, Office of Basic Energy Sciences, of the U.S. Department of Energy under Contract No. DE-AC02-05CH11231. Finally, we also would like to thank an anonymous reviewer for their comments.

APPENDIX
EXPERIMENTAL METHODS AND ANALYTICAL DETAILS

Sample Preparation and Irradiation

Gases were mixed at room temperature in a glass line evacuated by a diffusion pump (Edwards BRV 10, background pressure $\sim 5 \times 10^{-6}$ mbar). The starting mixtures included N_2 (gas, Matheson Tri-Gas, Matheson grade, 99.9995%), CH_4 (gas, Matheson Tri-Gas, Research purity, 99.999%), and either CO (gas, Scott Specialty Gases, CP grade, 99.99% purity) or $C^{18}O$ (gas, 95% ^{18}O, 99% purity) and were mixed in ~2-liter glass bulbs in a 100:1:1 ratio, to a total pressure of 102 mbar. The measured partial pressures were accurate to 0.05 mbar.

Experiments were performed inside a vacuum cryogenic chamber evacuated by a diffusion pump (Edwards BRV 25, background pressure $\sim 8 \times 10^{-8}$ mbar at room temperature. $\sim 2 \times 10^{-8}$ at 8–20 K). Pre-mixed gas mixtures were deposited onto a substrate cooled to 8–20 K by a closed-cycle helium cryo-cooler (APD Cryogenics) (Allamandola et al. 1988; Materese et al. 2014). With the exception of the experiments intended for XANES analysis, all ice mixtures were deposited on an ultra-high vacuum grade aluminum foil. The samples intended for XANES work were deposited on TEM grids coated with SiO films (SPI Supplies). The deposition of the gas onto the substrate led to the formation of a thin film of ice that was simultaneously irradiated with either a microwave-powered H_2-discharge UV lamp (Opthos) or a low-energy flood electron gun (EFG-8K, Kimball Physics). The H_2 lamp primarily emits photons mainly at 121.6 nm (Lyα) and also

produces a continuum centered around 160 nm, with an estimated total flux of $\sim 2 \times 10^{15}$ photons cm^{-2} s^{-1} (Warnek 1962). The electron gun was set to emit $\sim 1 \times 10^{15}$ e^{-} cm^{-2} s^{-1}, with an energy of 1.2 keV. Experiments yielding residues for GC-MS and IR spectroscopy typically lasted 70–90 hr and consumed 70–90 mbar of the initial gas mixtures used. Although we could not determine the thicknesses of the final ice films in these experiments, based on previous experiments, we estimate that they typically ranged from 12 to 15 μm (Materese et al. 2014). For XANES experiments, the simultaneous deposition and irradiation lasted only 20–24 hr and consumed 20–24 mbar of the initial gas mixture. These thinner samples were made to ensure that the resulting residues were thin enough such that their X-ray spectra would not be saturated.

At the conclusion of the deposition and radiation processing of each sample, the substrate was warmed by 1 K min^{-1} using a resistive heater to control the temperature up to a temperature of 150 K. Upon reaching 150 K, the cryo-cooler was shut off and the sample was allowed to warm to room temperature under a static vacuum.

Infrared Spectroscopy

Mid-IR (4000–600 cm^{-1}, 2.5–16.7 μm) and near-IR (7000–4000 cm^{-1}, 1.42–2.5 μm) spectra were collected independently at resolutions of 4 cm^{-1} and 8 cm^{-1}, respectively, using a Nicolet iN10 MX microscope. This microscope uses a liquid nitrogen-cooled mercury–cadmium–telluride (MCT) detector and a KBr beamsplitter. All the final spectra were ratioed against a background scan of the clean aluminum foil substrate. Mid-IR spectra were collected directly from the residues on the Al foils. However, these residues were not thick enough to produce appreciable absorption in the near-IR region in which overtones and combination modes usually show. Thus, in order to obtain high quality spectra in the near-IR region, the residues were dissolved in a 1:1 mixture of acetonitrile and methanol, and the solution was repeatedly spotted and dried onto a gold substrate to form a thicker sample layer. Mid-IR spectra were taken before and after the dissolution and spotting process to verify that there were no appreciable changes to the spectra of the residues due to the dissolution and re-deposition process.

XANES

XANES spectra were obtained with a scanning transmission X-ray microscope on beamline 5.3.2.2 at the Advanced Light Source (ALS) of the Lawrence Berkeley Laboratory, California, USA (Warwick et al. 2002; Kilcoyne et al. 2003). Following the same protocol as in Materese et al. (2014), the carbon (278–338 eV), nitrogen (385–419.5 eV), and oxygen (520–569.5 eV) edges, in addition to the full CNO scan range (278–584.5 eV) were collected using the line scan mode (10 μm lines, 100 points per line, 10-ms dwell times for each point). The relative abundances of carbon, nitrogen, and oxygen were obtained from full CNO scans using absorption coefficient curves (Henke et al. 1993). XANES data analyzed using the aXis 2000 software.

GC-MS

Samples intended for gas GC-MS analysis were transferred to pre-baked (500°C) glass vials containing 50 μL of a 3:1:1 mixture of *N*-(*tert*-butyldimethylsilyl)-*N*-methyltrifluoroacetamide (MTBSTFA) with 1% of *tert*-butyldimethylchlorosilane (*t*BDMCS) (Restek), dimethylformamide (Pierce, silylation grade solvent), and pyrene (Sigma-Aldrich, analytical standard, 100 ng μL^{-1} in cyclohexane). The vials were then heated to 100°C for 1 hr to convert hydrogen-bearing functional groups (e.g., OH and NH_2) to *tert*-butyldimethylsilyl (*t*BDMS) derivatives (MacKenzie et al. 1987; Casal et al. 2004; Schummer et al. 2009). Blank samples were also prepared to using the same protocols in order to identify any background contamination.

All GC-MS experiments were performed with a Thermo Trace gas chromatograph coupled to a DSQ II mass spectrometer. For each sample, 1 μL derivatized material was injected via syringe, using a splitless injection configuration with an injector temperature of 250°C. The stationary phase chosen was a Restek Rxi-5ms column (length: 30 m, inner diameter: 0.25 mm, film thickness: 0.50 μm). The mobile phase was helium (carrier gas, Airgas, ultra pure) with a flow rate of 1.3 mL $minute^{-1}$. The chosen temperature gradient is described in detail in Nuevo et al. (2009). Mass data were recorded from $m/z = 50$ to 550 Da. Data analysis utilized the Xcalibur™ software (Thermo Finnigan). Sample mass spectra were compared to the NIST database of mass spectra as well as our own database of retention times and mass spectra obtained from commercial standards.

REFERENCES

Allamandola, L. J., Sandford, S. A., & Valero, G. J. 1988, Icar, 76, 225
Baragiola, R. A., Famá, M. A., Loeffler, M. J., et al. 2013, in The Science of Solar System Ices, ed. M. S. Gudipati & J. Castillo-Rogez (Berlin: Springer), 527
Bohn, R. B., Sandford, S. A., Allamandola, L. J., & Cruikshank, D. P. 1994, Icar, 111, 151
Casal, S., Mendes, E., Fernandes, J. O., et al. 2004, J. Chromatogr. A, 1040, 105
Cody, G. D., Ade, H., Alexander, C. M. O'D., et al. 2008, M&PS, 43, 353
Cook, J. C., Cruikshank, D. P., & Young, L. A. 2014, in DPS meeting #46, Amer. Astron. Soc. #401.04 (abstract)
Cruikshank, D. P., Allamandola, L. J., Hartmann, W. K., et al. 1991, Icar, 94, 345
Cruikshank, D. P., Imanaka, H., & Dalle-Ore, C. M. 2005, Adv. Space Res., 36, 178
Cruikshank, D. P., Mason, R. E., Dalle Ore, C. M., et al. 2006, in DPS meeting #38, Amer. Astron. Soc. #21.03 (abstract)
De Gregorio, B. T., Sharp, T. G., Rushdi, A. I., et al. 2011, in Earliest Life on Earth: Habitats, Environments and Methods of Detection, Part 3, ed. S. D. Golding & M. Glikson (Netherlands: Springer Science), 239
DeMeo, F. E., Dumas, C., de Bergh, C., et al. 2010, Icar, 208, 412
d'Hendecourt, L. B., Allamandola, L. J., Grim, R. J. A., et al. 1986, A&A, 158, 119
Gerakines, P. A., Moore, M. H., & Hudson, R. L. 2001, JGR, 106, 33381
Gordon, M. L., Cooper, G., Morin, C., et al. 2003, JPCA, 107, 6144
Grundy, W. M., Olkin, C. B., Young, L. A., et al. 2013, Icar, 223, 710
Henke, B. L., Gullikson, E. M., & Davis, J. C. 1993, ADNDT, 54, 181
Hodyss, R., Howard, H. R., Johnson, P. V., et al. 2011, Icar, 214, 748
Hudson, R. L., Palumbo, M. E., Strazzulla, G., et al. 2008, in The Solar System Beyond Neptune, ed. M. A. Barucci et al. (Tucson, AZ: Univ. Arizona Press), 507
Imanaka, H., Khare, B. N., Elsila, C. M., et al. 2004, Icar, 168, 344
Imanaka, H., & Smith, M. A. 2010, PNAS, 107, 12423
Kilcoyne, A. D. L., Tyliszczak, T., Steel, W. F., et al. 2003, J. Synchrotron Rad., 10, 125
Kim, Y. S., & Kaiser, R. I. 2012, ApJ, 758, 37
Lellouch, E., Sicardy, B., de Bergh, C., et al. 2009, A&A, 495, L17
MacKenzie, S. L., Tenaschuk, D., & Fortier, G. 1987, J. Chromatogr. A., 387, 241
Madey, T. C., Johnson, R. E., & Orlando, T. M. 2002, SurSc, 5000, 838
Materese, C. K., Cruikshank, D. P., Sandford, S. A., et al. 2014, ApJ, 788, 111

Matthews, C. N. 1992, OLEB, 21, 421
Minard, R. D., Hatcher, P. G., Gourley, R. C., et al. 1998, OLEB, 28, 461
Moore, M. H., & Hudson, R. L. 2003, Icar, 161, 486
Nuevo, M., Milam, S. N., Sandford, S. A., et al. 2009, AsBio, 9, 683
Nuevo, M., Milam, S. N., Sandford, S. A., et al. 2011, AdSpR, 48, 1126
Palumbo, M. E., Ferini, G., & Baratta, G. A. 2004, AdSpR, 33, 49
Schummer, C., Delhomme, O., Appenzeller, et al. 2009, Talanta, 77, 1473
Stern, A. 2008, SSRv, 140, 3
Strazzulla, G., Baratta, G. A., & Palumbo, M. E. 2001, AcSpA, 57, 825
Vuitton, V., Bonnet, J.-Y., Frisari, M., et al. 2010, FaDi, 147, 495
Warnek, P. 1962, ApOpt, 1, 721
Warwick, T., Ade, H., Kilcoyne, A. D. L., et al. 2002, J. Synchr. Rad., 9, 254
Wu, Y.-J., Chen, H.-F., Chuang, S.-J., & Huang, T.-P. 2013, ApJ, 768, 83
Wu, Y.-J., Wu, C. Y. R., Chou, S.-L., et al. 2012, ApJ, 746, 175
Young, L. A., Stern, A., Weaver, H., et al. 2008, SSRv, 140, 93